Surface Science 268 (1992) 406–417
North-Holland

surface science

Phonons on fcc (100), (110), and (111) surfaces using Lennard-Jones potentials

I. Comparison between molecular dynamics simulations and slab technique calculations

D.D. Koleske and S.J. Sibener

The Department of Chemistry and The James Franck Institute, The University of Chicago, 5640 South Ellis Avenue, Chicago, IL 60637, USA

Received 20 September 1991; accepted for publication 18 November 1991

The surface phonon dispersion curves have been calculated for fcc (100), (110), and (111) surfaces using molecular dynamics (MD) simulations and Lennard-Jones pair potentials. In the low-temperature limit these MD simulations have been compared to the results from slab-technique lattice dynamics calculations of the type pioneered by Allen, Alldredge and de Wette. We compare the dispersion results between these two methods as a prelude to MD studies of the dispersion curves at elevated temperatures. At temperatures where the dynamical behavior is well described within the harmonic approximation, the two techniques should provide equal descriptions of surface phonon spectral densities and phonon frequencies. In this paper we demonstrate this agreement.

1. Introdution

Over the past twenty years, the surface phonon dispersion relations of many metals, insulators and semiconductors have been mapped over their entire surface Brillouin zones (SBZ) using electron energy loss spectroscopy (EELS) and helium atom scattering (HAS) [1]. To provide a physical interpretation of the experimental data, many lattice dynamics models have been constructed, spanning the range from simple force constant models [1,2] to ab initio methods [3]. Above all, these experimental and theoretical studies clearly indicate that the surface force field can differ substantially from that of the bulk [1].

Once a dynamical model is developed to describe the surface vibrational behavior, various methods can be used to calculate the surface phonon dispersion, which then can be compared to the experimentally measured curves. One frequently used method is the slab technique (ST), developed over twenty years ago by Allen, Alldredge and de Wette [4–6]. Using the ST, a microscopic understanding of the surface vibrations can be developed since the dispersion curve frequencies are calculated directly, along with the polarization vectors and the vibrational amplitudes of the modes. This is possible because the dynamical matrix is solved for a finite number of layered slabs of atoms, and the resulting eigenvector's displacement and its corresponding eigenvalue can be assigned to a particular slab layer. Another method is the Green's function (GF) technique, which treats the surface lattice dynamics as a perturbation of the bulk lattice dynamics [7]. A GF calculation of the surface dynamical behavior yields information on the surface phonon density of states and clear discrimination between "true" surface localized modes and surface resonances. This technique is also favored when calculating defects in a lattice since the defects can usually be treated as an additional perturbation. A third method which has not been used as extensively is molecular dynam-

ics (MD) simulations [8–11]. Here the atoms move according to Newton's laws of motion, where the force acting on each atom is obtained by summing the component forces from surrounding atoms. Using this method, the surface spectral densities can be obtained by Fourier transforming the velocity–velocity or displacement–displacement autocorrelation functions [8–12]. Since this method allows one to study vibrations at finite temperatures, it can be applied to study temperature dependent phenomena, such as anharmonic effects on surface dynamics [13–18], soft-mode driven phase transitions [9–11,19,20], and surface melting and disordering [21–26].

Each of these three techniques has advantages and disadvantages when used for calculating surface vibrations. Typically the ST and GF methods are preferred, since the surface phonon frequencies and spectral densities can be obtained without too much computational effort. However, using the ST to calculate the dynamical properties of stepped surfaces or surfaces with several basis atoms becomes computationally cumbersome because large matrices are needed for convergence of the eigenvectors and eigenvalues. For example, an early study of stepped Ni surfaces needed to use many slab layers in order for the slab modes to converge in frequency [27]. This computational difficulty arises because inverting the dynamical matrix to find both the eigenvalues and eigenvectors typically involves $3N^3$ operations per Q-vector, where N is the dimensionality of the matrix [28]. ST methods have been developed for stepped surfaces where the dynamical matrix is solved on a computer using a symbolic algebra routine, but even this simplification requires significant computational effort [29]. On the other hand, the matrix used in GF calculations does not grow in size as dramatically as the size of the system increases. In Knipp's calculations of high-Miller-index surfaces, the matrix dimensionality increased proportionately to the number of terrace atoms [30]. However, GF methods become increasingly difficult when more than first nearest neighbor interactions are considered. Furthermore, in order to describe vibrational characteristics at higher temperatures, such as changes in the phonon frequency and linewidth, GF calculations must include perturbative terms for the virtual phonon–phonon interactions [31–34], requiring further computational effort.

MD simulations require significantly more computational effort when compared to ST and GF calculations when used for calculating the lattice dynamics at low temperature. This effort is required because the force acting on each atom from the shells of neighboring atoms must be calculated at each time step, and many time steps are typically needed for sufficient resolution of the features in the surface phonon spectral density. The computational expenditure for calculating the force on each atom from the surrounding atoms goes as the square of number of nearest neighbors included in the force sum. This implies that the dynamics of very large systems might be better solved using MD simulations than using the ST or GF methods. The advantage of using MD simulations is that the temperature dependence of phonon modes can be calculated directly. Elevated temperature effects on surface phonon dynamics form the subject of the following paper (paper II) as well as that for subsequent work on stepped and basal surfaces using LJ and Finnis–Sinclair potentials [35,36]. One of the disadvantages of this technique is that only certain values in reciprocal lattice can be simultaneous sampled. This disadvantage can be overcome by using differently sized surfaces to fill in the wavevector dependence of the dispersion relations. Another disadvantage of the MD method is that only the spectral density is calculated, therefore the actual atomic displacement of the vibrational mode can only be inferred from the polarization of the calculated spectral densities.

In this paper we concentrate on using low-temperature MD simulations and LJ pair potentials to calculate the surface phonon spectral densities for fcc (100), (110), and (111) surfaces. These MD results will then be compared with those calculated using the ST. We first discuss general characteristics of the MD technique we used, including lattice constant selection, equilibration criteria, and how the surface phonon spectral densities were calculated. We then briefly discuss how the ST calculations were carried out. We report the results of the low-temperature simulations,

and discuss the criteria used to determine when equilibrium is reached. Interesting temperature fluctuations which are due to the finite size of the system are also presented. Finally, we compare the dispersion relations obtained using MD and ST methods, and compare the calculated spectral densities at one wavevector for the (110) surface.

2. Background

In this section we present the equations and methods which we have used for calculating the surface phonon dispersion relations for the three basal planes of fcc crystals. The formalism we use for calculating the surface phonon dispersion relations from MD simulations has been drawn from previously published work [8–13,16,37,38]. We outline the technique and equations used for transforming the velocity vectors of the surface atoms into the surface phonon spectral densities. We also present the slab technique equations from which we calculated the surface phonon dispersion relations and surface spectral densities that were later compared to the MD simulation results.

2.1. Molecular dynamics simulations

To obtain the surface phonon spectra, Newton's equation of motion, $\vec{F} = m\vec{a}$, is integrated. The integration of this equation should use the largest time step possible while still maintaining good total energy conservation. We find that a 7th-order predictor–corrector (PC) algorithm satisfies these two requirements [39]. Generally, using PC's with orders greater than 7 do not increase the accuracy of the calculation nor the maximum time step that can be taken [40]. We found that using PC's of orders less than 7 substantially increased the numerical error from increases in the time step [40]. One good check of overall efficiency of the integrator is to monitor the total energy during the simulation, which should ideally maintain a constant value. The energy drain, defined as the rate at which the total energy drops during the simulation, using a 5th-order PC was typically 50–100 times greater than if a 7th-order PC was used. For all simulations reported here a total energy drain of no more than $2.0 \times 10^{-4}\%$ occurred over the 4096 time steps collected for generating each phonon spectrum.

The force $\boldsymbol{F}_i$ acting on the ith atom is a sum of the component forces acting on the ith atom, and is given by,

$$\boldsymbol{F}_i = m_i \frac{\partial^2 \boldsymbol{r}_i}{\partial t^2} = \sum_{j \neq i}^{N} \boldsymbol{F}_j = -\sum_{j \neq i}^{N} \frac{\boldsymbol{r}_{ij}}{|\boldsymbol{r}_{ij}|} \frac{\partial V(r_{ij})}{\partial r_{ij}}, \quad (1)$$

where bold letters designate vectors, m_i is the mass, and $\boldsymbol{r}_i$ is the position coordinate. The component forces $\boldsymbol{F}_j$ are found by differentiating a scalar potential multiplied by the magnitude of the force acting in the $\hat{x}$, $\hat{y}$, or $\hat{z}$ direction. We have used a Lennard-Jones (LJ) 6–12 potential for all calculations in this paper, which is given by:

$$\phi(r_{ij}) = 4\epsilon\left[\left(\frac{\sigma}{r_{ij}}\right)^{12} - \left(\frac{\sigma}{r_{ij}}\right)^{6}\right]. \quad (2)$$

It is well understood that LJ potentials do not accurately model metals or semiconductors [37]. However, they have a simple analytical form and surface phonon dispersion curves have been calculated for LJ solids using the ST methods [5]. The total potential energy of the simulated solid, P_{tot}, is equal to

$$P_{\text{tot}} = \tfrac{1}{2} \sum_{i=1}^{N} \sum_{j=1}^{\text{NN}} \phi(r_{ij}), \quad (3)$$

where i is summed over all atoms in the simulation, N, and j is a sum over the shell of interaction neighbors, NN.

When using Lennard-Jones potentials the lengths and the time can be expressed in dimensionless units $S = r/\sigma$ and $\tau = t/(M\sigma^2/\epsilon)^{1/2}$ [5]. With these substitutions, the equations of motion then become [5]:

$$\frac{\partial^2}{\partial^2 \tau} S_i^{\alpha} = 24 \sum_{j}^{\text{NN}} \frac{S_i^{\alpha} - S_j^{\alpha}}{S_{ij}^{8}} \left[2\left(\frac{1}{S_{ij}^{6}}\right) - 1\right], \quad (4)$$

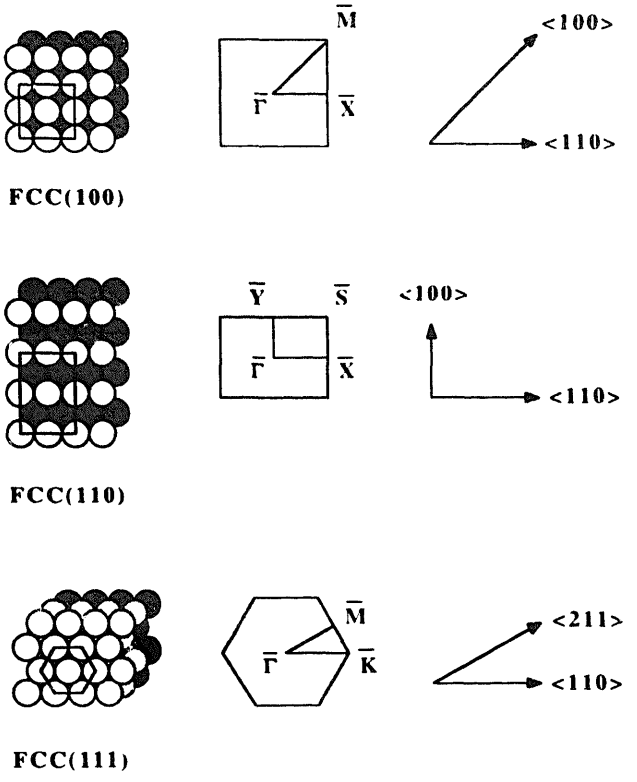

Fig. 1. Plotted in the left hand column are the geometric arrangement of atoms for fcc (100), (110), and (111) surfaces. In the middle column the reciprocal lattice or surface Brillouin zone corresponding to each direct lattice is shown. On the right-hand side are plotted the major directions in the surface plane. These are the same geometries and directions used by Allen, Alldredge and de Wette [5].

where S_{ij} is given by:

$$S_{ij} = \left[\sum_{\alpha} (S_i^{\alpha} - S_j^{\alpha})^2 \right]^{1/2}, \tag{5}$$

and the sum α is over the three components of motion.

At the start of each simulation, the initial conditions of the parallelepiped slab are established, two sides of which are free surfaces. The remaining four sides are surrounded by periodic boundary conditions [37]. The surface geometries and directions used in this study are shown in fig. 1. The $\hat{x}$ unit direction is always chosen so that the surface atoms are only one atomic spacing, a, apart from each other. The $\hat{y}$ unit direction is chosen to be $\hat{y} = a$ for the (100); $\hat{y} = (\sqrt{2})a$ for the (110); and $\hat{y} = (\sqrt{3}/2)a$ for the (111). The $\hat{z}$ unit direction is chosen to be normal to the surface.

At every temperature, T^*, where $T^* = (m/k_B)T$, the lattice constant a must be set to account for the thermal expansion of the lattice. The lattice constant is set to establish the periodic boundary length which is held constant during the simulation. This allows interplanar expansion of the lattice normal to the surface plane, but keeps the intraplanar lattice spacing fixed. The lattice constant is set at each T^* to account for the bulk thermal expansion and is described by the functional form, $a = c_0 + c_1 T^* + c_2 T^{*2}$, where $c_0 = 1.0903\sigma$, $c_1 = 0.0295\sigma$, and $c_2 = 0.072\sigma$. This functional form has been chosen since it well describes the thermal expansion of the heavier rare gas solids [41]. The values of c_0, c_1, and c_2 were obtained by fitting the lattice constant a at three temperatures, $a = 1.14$ at $T^* = 0.655$ [37], which is the melting temperature, $a = 1.115$ at $T^* = 0.30$ [38], and $a = 1.0903$ at $T^* = 0.0$, which is obtained by minimization of the bulk potential energy.

Since more than 95% of the program run time is spent calculating the force sums, it is desirable to calculate them efficiently at every time step over all atoms where the interaction is significant. To expedite these force sum calculations, a table of neighboring atoms is calculated out to a particular radius around each atom. In this paper, r_c is set to include a maximum of 176 atoms (9 shells of interactions), or $r_c = 3.0a$. Any atom beyond this radius contributes only a 0.0142% increase to the total potential energy, and a negative force of $F_i = -0.004\,139\epsilon/\sigma$ as compared to the force at $r_c = a$, which is $F_i = 8.376\epsilon/\sigma$. This table decreases the total computational time needed because only the forces orginating from atoms at less that the cutoff radius, r_c, are calculated during each time step, rather than using all atoms that comprise the solid.

The simulation temperature is chosen by scaling the velocities of the system [37]. The temperature $T^* = (m_i/k_B)T$ of the system is related to the velocities of the atoms by:

$$T^* = \frac{1}{3N} \sum_{i=1}^{N} \sum_{\alpha}^{3} \langle \dot{S}_i^{\alpha 2} \rangle, \tag{6}$$

where S_i^α denotes the first derivative of the scaled position, S_i^α, with respect to time. A Maxwellian distribution of velocities is assigned randomly to the ensemble of atoms, except for one bulk atom which is not assigned. This atom's velocity is assigned with the constraint that the sum of the crystal momentum be zero. After the velocities are assigned, the temperature of the ensemble is calculated and the velocities are then scaled to match the assigned temperature.

For a Maxwellian distribution in three dimensions, thermal equilibrium is attained when $\alpha(\tau)$, which is:

$$\alpha(\tau) = \frac{(1/N)\sum_{i=1}^{N}\sum_{\alpha}^{3}\{\dot{S}_i^\alpha(\tau)^2\}^2}{\left((1/N)\sum_{i=1}^{N}\sum_{\alpha}^{3}\dot{S}_i^\alpha(\tau)\right)^2} \tag{7}$$

equals 5/3 [37,42]. Because a finite number of atoms are simulated, $\alpha(\tau)$ fluctuates around 5/3 and the fluctuations are of order $1/\sqrt{N}$ [42]. The quantity $\alpha(\tau)$, along with T^*, potential energy, P^*, and total energy, E^*, of the whole ensemble are stored and can be checked during the simulation. Also stored for each time step are the temperatures of both free surfaces. The integration of the differential equations then proceeds for about 2000 time steps. At the conclusion of this integration time, the simulation ensemble is considered to be in equilibrium because $\alpha(\tau) = 5/3$, and both free surfaces have reached the simulation temperature. Surface phonon spectral densities taken after this number of time steps yield essentially identical spectra.

When equilibrium is reached, the integration continues for 4096 time steps and the two-dimensional Q-resolved velocity vectors are stored. These velocity vectors, $\dot{S}^\alpha(Q; l_z)$ are given by

$$\dot{S}^\alpha(Q; l_z) = \sum_j \dot{S}^\alpha(j; l_z)\exp[iQ\cdot S(j; l_z)], \tag{8}$$

and are obtained by taking the discrete 2D Fourier transform (FT) of the j atoms in the l_zth plane. In eq. (8), Q is a wavevector parallel to the surface, and $S(j; l_z)$ is the current position of the jth atom in the l_zth layer. Since the surface contains a finite number of atoms, only integral values of the FT Q-vectors are accessible. This is because the $n \times n$ 2D surface positions are real, and the corresponding 2D FT of these positions gives $\frac{1}{2}n + 1$ unique Q-vector values.

At the program's completion the Q-resolved velocity vectors $\dot{S}^\alpha(Q; l_z, \tau)$ are transformed to yield the phonon spectral density functions $g^{\alpha\beta}(Q; l_z, \omega)$. The spectral density function is the FT of the velocity–velocity autocorrelation, and is given by

$$g^{\alpha\beta}(Q; l_z, \omega) = \int_{-\infty}^{\infty} d\tau \exp(i\omega t) \times \frac{\langle \dot{S}^\alpha(Q; l_z, \tau)\dot{S}^\beta(Q; l_z', 0)\rangle}{\langle \dot{S}^\alpha(Q; l_z, 0)\dot{S}^\beta(Q; l_z', 0)\rangle}. \tag{9}$$

To evaluate $g^{\alpha\beta}(Q; l_z, \omega)$, we take advantage of the correlation theorem, which replaces the double sum needed for the correlation in the time domain with one complex multiplication in the frequency domain [28]. This method is also faster when the FT are performed using a fast-FT (FFT) algorithm [28]. The Q-resolved velocity vectors, $\dot{S}^\alpha(Q; l_z, \tau)$, are FFTed and the corresponding correlation function found by multiplying $\dot{S}^\alpha(Q; l_z, \omega)$ by the complex conjugate $S^\beta(Q; l_z, \omega)^*$. This product is then back-transformed to the time domain and the product normalized by the denominator in eq. (9) to obtain the autocorrelated functions. The correlation function $g^{\alpha\beta}(Q; l_z, \tau)$ is then FFTed again to get $g^{\alpha\beta}(Q; l_z, \omega)$.

The spectral density $f^{\alpha\beta}(Q; l_z, \omega)$ shown in all figures is obtained by taking the power spectrum of $g^{\alpha\beta}(Q; l_z, \omega)$. For the time step we used, h, an energy resolution of $\Delta\omega_{res} = 2\pi/(h \times 4096)$ is achieved, where the frequency, ω, is in units related to the LJ potential by $\omega = \sqrt{\epsilon/M\sigma^2}$ [5]. In this paper, $h = 0.008\tau$, which corresponds to a frequency resolution of $\Delta\omega_{res} = 0.1917\omega$. The surface phonon spectra for both free surfaces are then added together.

All MD spectral densities $f^{\alpha\beta}(Q; l_z, \omega)$ are shown as calculated, i.e., no Gaussian filtering was used [38]. The spectral densities are the sum of 4 averaged simulation runs taken from consecutive runs. Upon completion of the simulation,

the atomic positions were checked to make sure that they had not moved out of their assigned lattice positions.

2.2. Slab calculations

The low-temperature ($T^* = 0.02$) phonon spectral densities and frequencies obtained from the MD simulations discussed above were compared to spectral densities and frequencies obtained using the ST as originally described by Allen, Alldredge and de Wette in their pioneering study of surface phonons [5]. Before calculating the dynamical properties of the lattice with the ST the slab layers were first allowed to relax, until the net force acting on each slab layer was zero. This process was repeated in a consistent manner until the layer relaxations converged.

The ST calculation gives the eigenvalues $\omega^\alpha(\boldsymbol{Q}; l_z)^2$ and eigenvectors $e^\alpha(\boldsymbol{Q}; l_z)$ of the dynamical matrix $D^{\alpha\beta}(\boldsymbol{Q}; l_z, l_z')$ as a function of $\boldsymbol{Q}$;

$$\omega^\alpha(\boldsymbol{Q}; l_z)^2 e^\alpha(\boldsymbol{Q}; l_z) = \sum_{l_z'\beta} D^{\alpha\beta}(\boldsymbol{Q}; l_z, l_z') e^\beta(\boldsymbol{Q}, l_z'), \quad (10)$$

where $D^{\alpha\beta}(\boldsymbol{Q}; l_z, l_z')$ for a one component system is given by:

$$D^{\alpha\beta}(\boldsymbol{Q}; l_z, l_z') = \{M\}^{-1} \sum_{l_z' j'} \Phi^{\alpha\beta}(l_z, j; l_z', j') \times \exp(\mathrm{i}\boldsymbol{Q} \cdot \{\boldsymbol{R}_0(j; l_z) - \boldsymbol{R}_0(j', l_z')\}). \quad (11)$$

The dynamical matrix $D^{\alpha\beta}(\boldsymbol{Q}; l_z, l_z')$ is the layer-by-layer 2D FT of the force constant matrix $\Phi^{\alpha\beta}(l_z, j; l_z', j')$, and is related to the first and second derivatives of the LJ(6–12) pair potential by

$$\Phi^{\alpha\beta}(l_z, j; l_z', j') = -\frac{S_{jj'}^\alpha S_{ij'}^\beta}{S_{j'}^2}\left(\phi''(S_{jj'}) - \frac{1}{S_{jj'}}\phi'(S_{jj'})\right) + \frac{\delta^{\alpha\beta}}{S_{jj'}}\phi'(S_{jj'}). \quad (12)$$

When $l_z = l_z'$ and $j = j'$ in eq. (11), the value of $\Phi^{\alpha\beta}(l_z, j; l_z', j')$ is equal to the negative sum over the l_z'th and j'th atoms. This is the self-interaction term and is added to the other terms in eq. (11). Since in this term the positions $\boldsymbol{R}_0(j; l_z)$ and $\boldsymbol{R}_0(j', l_z')$ are identical, the exponential term in eq. (11) is zero. This term is the restoring force on the jth atom in the l_zth layer from the rest of the lattice [43]. A detailed formula for $D^{\alpha\beta}(\boldsymbol{Q}; l_z, l_z')$ using a LJ(6–12) potential was previously derived by Allen and de Wette [44]. The square root of the eigenvalues $\omega^\alpha(\boldsymbol{Q}; l_z)$ are plotted as a function of $\boldsymbol{Q}$ for the three surfaces studies and are shown in ref. [5] and are shown later in this paper in figs. 7–9.

In addition to calculating the energies of the modes, the layer-by-layer spectral densities can also be calculated by:

$$\rho^{\alpha\beta}(\boldsymbol{Q}; l_z, \omega) = \sum_n e^\alpha(\boldsymbol{Q}; l_z) e^\beta(\boldsymbol{Q}; l_z')^* \delta(\omega - \omega_n). \quad (13)$$

The spectral densities $\rho^{\alpha\beta}(\boldsymbol{Q}; l_z, \omega)$ for a given $\boldsymbol{Q}$ were obtained by multiplying the layer-by-layer eigenvectors by a Lorentzian whose width was equal to the time resolution of the MD simulation. The spectral densities obtained via MD simulations and slab calculations have recently been shown to be identical within the harmonic approximation [45]. Similar agreement has already been demonstrated for surface spectral densities obtained using the ST and GF methods for O on Ni(111) [46].

3. Simulation results and discussion

The low-temperature simulations, $T^* = 0.02$, were performed mainly to confirm that the molecular dynamics program was working correctly. At this T^*, the atoms vibrate near their equilibrium lattice positions and their dynamics can be described within the harmonic approximation [37]. Schommers has stated that anharmonic contributions to the dynamics in LJ solids should become important when $T^* = \frac{1}{3}T_m^*$ in the bulk and at $T^* = \frac{1}{6}T_m^*$ at the surface [37]. At $T^* =$

0.02, which is 3.1% of the bulk melting temperature of LJ solids, anharmonic effects should be negligible and the two methods, MD and SC, should give identical results.

During the simulations we monitored the intrinsic properties, such as temperature and total potential energy, of the atomic ensemble. The temperature T^* versus time for a (100) surface at $T^* = 0.02$ is plotted in fig. 2 for a $12 \times 12 \times 41$ (i.e., $l_x \times l_y \times l_z$) dimensioned slab. At the start of the simulation, T^* is set to twice the desired kinetic energy ($T^* = 0.04$). As the simulation proceeds, T^* drops and fluctuates about $T^* = 0.02$. At $\tau = 0$, P_{tot} (defined in eq. (3)) is equal to P_{lat}, and this value of P_{tot} is the lowest that occurs during the simulation. The dynamical potential energy, P^*, which is plotted in fig. 2, is the difference between these two potential energies, or $P^* = P_{tot} - P_{lat}$. As can be seen in fig. 2, P^* fluctuates about 0.02 as is expected from the equipartition of energy. Also plotted in fig. 2 is the total energy of the system $E^* = P^* + T^* = 0.04$. The total energy E^* should remain constant throughout the entire simulation. However, it slowly and continuously drops during the simulation, due to numerical error of the integrator. This drop in E^* is insignificant, and is less than $1 \times 10^{-4}\%$ of the total energy. The simulation statistics are not influenced by this drop in E^*,

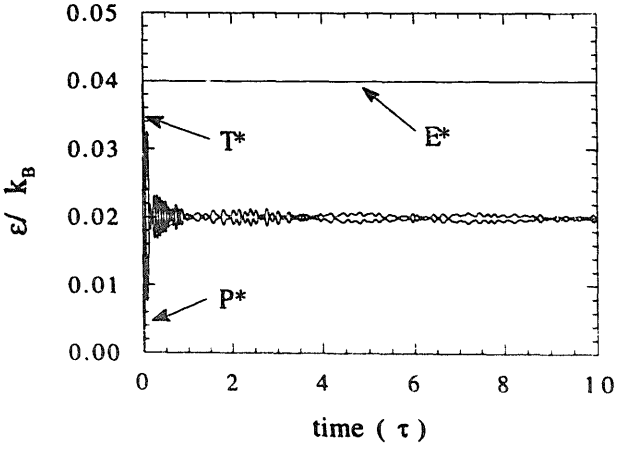

Fig. 2. Plot of the temperature, T^*, versus time for a (100) surface with dimensions of $(12 \times 12 \times 41)$. The simulation temperature is $T^* = 0.02$. The time dependence of the potential energy P^* and the total energy E^* are also plotted. Note that $E^* = T^* + P^*$.

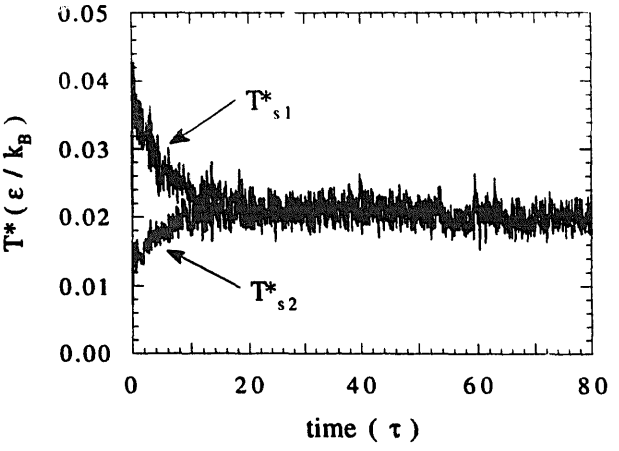

Fig. 3. Plot of the two surface temperatures T_{s1}^* and T_{s2}^* versus time for a 41-layer thick slab, with a 12×12 dimensioned (100) surface.

nor does the simulation temperature noticeably decrease.

In fig. 3 the two surface temperatures T_{s1}^* and T_{s2}^* are plotted versus time (the subscript s1 refers to the top layer and s2 refers to the bottom layer). T_{s1}^* starts off at a higher temperature than T_{s2}^*, which is due to how the initial coordinates and second derivatives are iteratively solved at the start of the simulation. These iterative solutions are solved starting from the top surface layer, proceeding through the bulk, and finishing with the bottom surface layer. After about 1000 time steps, both surfaces achieve the same surface temperature to within the random noise fluctuations.

Plotted in fig. 4 is the value of $\alpha(\tau)$ as a function of time. As the simulation proceeds, $\alpha(\tau)$ approaches the value of 5/3, which is shown in fig. 4 as a solid horizontal line. The distribution of $\alpha(\tau)$ is Gaussian and has a standard deviation of 0.023, about 75% greater than $(1/\sqrt{N})$. This deviation larger than $(1/\sqrt{N})$ in $\alpha(\tau)$ is due to fluctuations which will be discussed shortly. Equilibrium was assumed to be achieved when $\alpha(\tau) = 5/3$ and when the surface temperatures T_{s1}^* and T_{s2}^* fluctuated around the simulation temperature. Simulations calculated under these conditions produced spectra that had the same surface phonon frequencies and intensities.

A closer examination of T^* for longer total integration times shows that the temperature

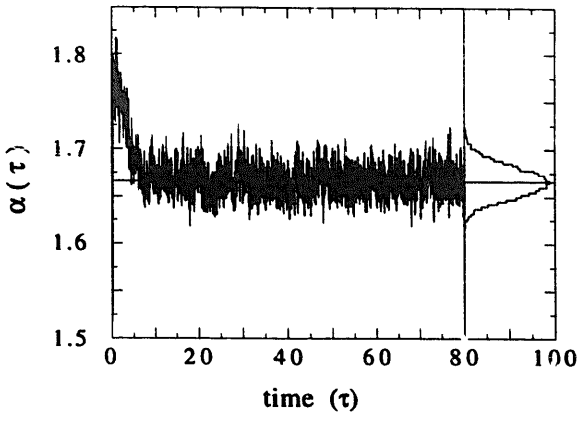

Fig. 4. Plot of $\alpha(\tau)$ versus time. As described in the text $\alpha(\tau)$ fluctuates about 5/3, which is shown in the figure by a solid horizontal line. The distribution of values for $\alpha(\tau)$ is shown from $\tau = 10$–80.

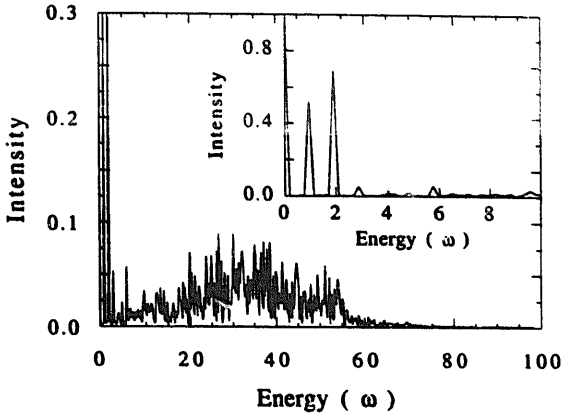

Fig. 6. The frequency spectrum for the 41-layer simulation from fig. 5. In the inset is a blowup of the low-frequency region of the spectrum, which shows that these frequencies correspond to the $\hat{z}$-component of motion phonon frequency at $\bar{\Gamma}$ and its first harmonic.

fluctuates periodically, and that this fluctuation depends on the thickness of the MD slab. In fig. 5 T^* values from three different simulations each with approximately the same number of particles, but with different slab thicknesses, are plotted. As the slab thickness was increased the time between these fluctuations increased linearly at a rate of 0.156τ per slab layer. The frequency spectrum of T^* for the $12 \times 12 \times 41$ simulation is shown in fig. 6, and the inset is a blowup of the low-frequency region of this spectrum. Two low-frequency features appear, one at a frequency equal to 1.0ω and a second equal to 2.0ω, which is the first harmonic of the first. At higher temperatures ($T^* = 0.10$) the 2nd harmonic (3.0ω) of this frequency was also observed. (Further investigation of the possibility of observing still higher harmonics were not conducted). These low-frequency modes correspond to the time between the oscillations that occur in fig. 5, *and have the same frequency as the $\hat{z}$-polarized phonon mode at the zone origin (i.e., $\bar{\Gamma}$)*. The temperature fluctuations observed in fig. 5 are due to low-frequency motions of the entire slab. Other than increasing the intensity of the $\bar{\Gamma}$ mode, the oscillation of T^* does not seem to influence the shorter wavelength modes, since the surface temperature, T_{1s}^* and T_{2s}^*, do not show this oscillation. Any influence that this oscillation may have on the modes near the zone origin is not considered further, since these modes are not calculated accurately by either the ST or MD due to the finite sizes of the computed systems.

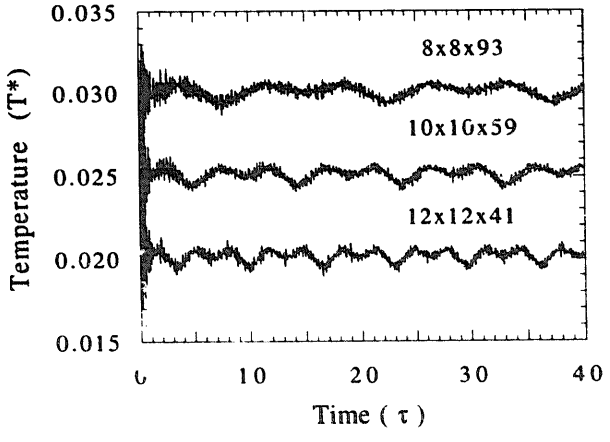

Fig. 5. T^* is plotted for three simulations, each with approximately the same number of particles, but with different slab thickness. Top panel: 93 layers; middle panel: 59 layers; and bottom panel: 41 layers. For each simulation $T^* = 0.02$. The top two simulation temperatures have been offset by 0.05 and 0.10, respectively.

If a larger value of the lattice constant ($a = 1.093$) is used in the simulations at $T^* = 0.02$, these long wavelength oscillations disappear. The reason these oscillations disappear can be understood by noticing that the surface atomic spacing, set at the start of the simulation, is smaller than the atomic spacing that would be calculated by minimizing the potential energy at the surface. This is an effect due to the change in the number

of nearest neighbors which occurs at the surface. For example, the minimum in potential energy for a two-atom system occurs at an interatomic separation of 1.122σ; the minimum in potential energy for a two-dimensional hexagonal sheet of atoms occurs at an interatomic separation of 1.115σ; and for a bulk three-dimensional crystal it occurs at a lattice separation of 1.0903σ. During the simulation, the interlayer spacing increases normal to the surface plane to lower the potential energy of the simulation ensemble. However, the periodic boundary conditions that are established at the start of the simulation lock the intraplanar atomic positions to the bulk intraplanar atomic positions. A motion which bows the surface outward would increase both the interlayer and the intralayer lattice spacing and subsequently reduce the potential energy of the entire ensemble. This motion would be similar to the displacements of a Rayleigh wave at $\bar{\Gamma}$. The temperature oscillations observed in fig. 5 coincide with these potential oscillations, since $T^* = E^* - P^*$, where E^* is constant.

The MD spectral density peaks are shown as open circles for the (100) surface in fig. 7, for the (110) in fig. 8, and for the (111) in fig. 9. The phonon frequencies obtained using the ST method are also plotted in figs. 7–9 as solid lines. The $\omega^{\alpha}(\boldsymbol{Q}; l_z)$ for these figures were obtained using 41 slab layers with a cutoff radius of 176

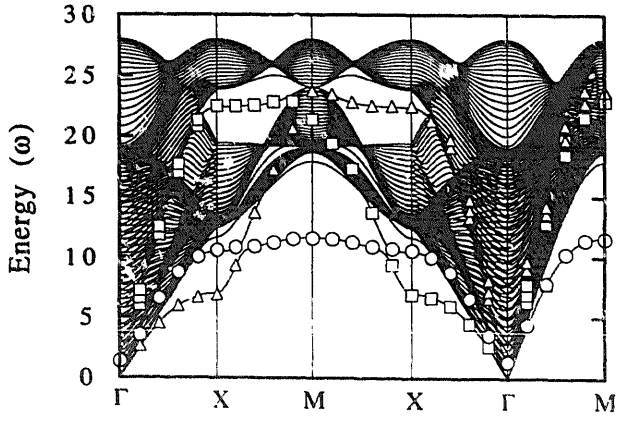

Fig. 7. Comparison of the peaks obtained from the $T^* = 0.02$ MD spectral density functions for the (100) surface in all three directions: $\hat{x}$ = □ panel, $\hat{y}$ = △, and $\hat{z}$ = ○. A 10×10 arrangement of surface atoms was used, which corresponds to a 6×6 $\boldsymbol{Q}$ vector sampling of the surface phonons.

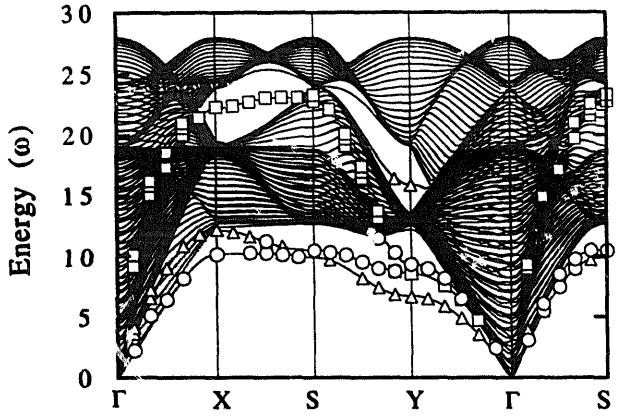

Fig. 8. Same as fig. 7, except for the (110) and a 12×12 arrangement of surface atoms, which results in a 7×7 $\boldsymbol{Q}$ vector sampling of the surface phonons.

NN, with the matrix diagonalization performed at 20 equally spaced $\boldsymbol{Q}$ values between the high-symmetry points. The spectral peaks that are plotted are the major peaks in the $\hat{x}$–□, $\hat{y}$–△, and $\hat{z}$–○ autocorrelated spectral densities, $f^{\alpha\beta}(\boldsymbol{Q}; l_z, \omega)$. The MD simulation size for the (100) and (111) surfaces was $10 \times 10 \times 31$, and the size for the (110) surface was $12 \times 12 \times 41$. This gives reciprocal space dimensions of 6×6 for the (100) and (111), and 7×7 for the (110). The MD results are in excellent agreement with the ST calculations in frequency. The directional components of the vibrations also agree well with the ST calculated ones as first reported by Allen, Alldredge and de Wette [5]. In particular, the S_1 mode's spectral density at $\bar{X}$ on the (100) surface has mainly a $\hat{y}$-component of motion which agrees

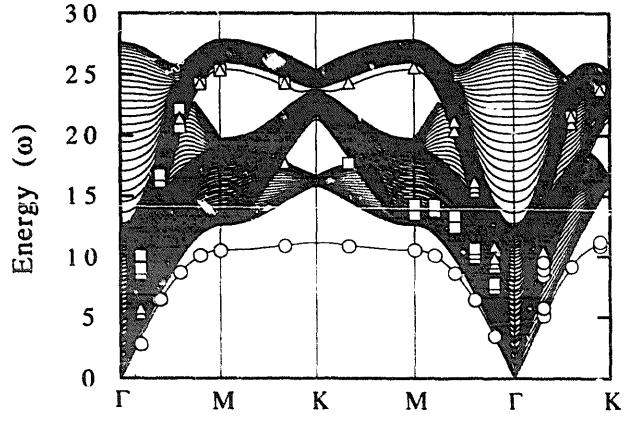

Fig. 9. Same as fig. 7, except for the (111) surface.

with the shear horizontal character of this mode. Another example of this agreement between the MD and ST is the switch that occurs in the directional component of the S_1 mode on the (110) surface, from a $\hat{z}$-component of motion near $\bar{X}$ to a $\hat{y}$-component between $\bar{X}$–$\bar{S}$ [5].

To check for size effects on the calculated phonon modes, various differently sized simulations for a LJ(100) surface were tried. Even for the smallest simulation with ensemble dimensions of $6 \times 6 \times 21$, no change was observed in the calculated frequencies of the short wavelength modes (i.e., near $\bar{X}$ and $\bar{M}$). However, as the number of layers in the ensemble was reduced the frequency of the $\bar{\Gamma}$ mode increased in frequency at the rate of 0.028ω per layer. For an infinitely thick ensemble the frequency of the $\bar{\Gamma}$ mode equals zero, but does not in our simulations because the ensemble thickness is finite.

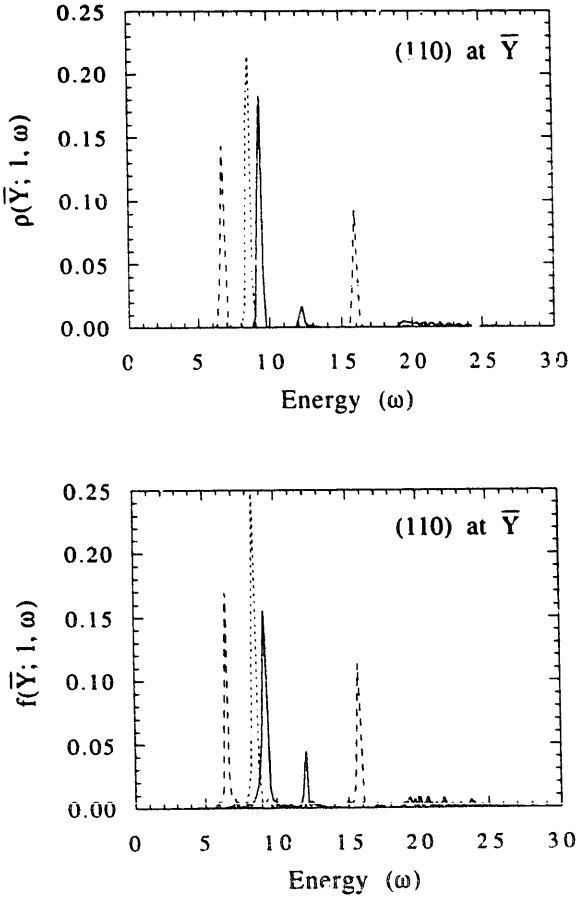

Fig. 10. This plot compares the spectral densities obtained from ST calculations (upper panel) and from MD simulations (lower panel) for the $\bar{Y}$ modes on a (110) surface. The $\hat{x}$ direction is the short-dashed line, the $\hat{y}$ direction is the long-dashed line, and the $\hat{z}$ direction is the solid line.

A plot comparing the spectral density functions calculated by MD, eq. (8), and ST, eq. (13), for the $\hat{x}$, $\hat{y}$, and $\hat{z}$ polarizations are shown in the upper and lower panels of fig. 10, respectively. The spectral densities plotted in fig. 10 were obtained for the (110) surface at $\bar{Y}$. The MD frequency resolution shown in fig. 10 is $\Delta\omega_{res} = 0.1917\omega$. This resolution was used in the corresponding ST calculations in order to facilitate comparison of the spectral densities generated by the two methods. In fig. 10, the MD simulation freqencies are slightly red-shifted from the ST calculations. This discrepancy is due to the difference in the interlayer expansion of the lattice, which was slightly larger in the MD simulations than in the ST calculations [13]. Because the MD interlayer spacings are larger, the effective force constant between the first and second layer will be reduced, thereby lowering the phonon frequency. Despite this small discrepancy, the overall agreement in both frequency and intensity of the modes between these two methods is excellent. The spectral densities obtained using the ST and MD techniques also show excellent agreement for the LJ(100) surface at $\bar{X}$ and for LJ(111) surface at $\bar{M}$ but are not shown.

4. Conclusions

In this paper we have demonstrated that the surface phonon frequencies and spectral densities calculated using MD simulations agree well with the results obtained using the ST for temperatures where the lattice dynamics is described within the harmonic approximation. We have outlined the process used to calculate the surface phonon spectral densities using MD simulations. Particular attention has been paid to the intrinsic properties of the ensemble of atoms during the simulations in order to ensure that the surface phonon spectral densities are taken for an equilibrated ensemble. Our results indicate that once a model potential is developed the lattice dynamics

can be well described using MD simulations for comparison with experiment.

The real power of MD simulations lies in the ability to calculate the temperature dependence of the surface phonon features. This will be especially important as we seek to develop a better understanding of how anharmonicity influences surface dynamical behavior as the temperature is increased. Results from elevated temperature simulations will be presented in paper II of this series.

Acknowledgements

We wish to acknowledge many helpful conversations with P.A. Knipp. We also thank D. Mills, D.F. Padowitz, L. Brown, S.F. King and T. Curtiss. This work was supported, in part, by the Air Force Office of Scientific Research and the National Science Foundation Materials Research Laboratory at The University of Chicago.

References

[1] W. Kress and F.W. de Wette, Surface Phonons, Springer Series in Surface Science Vol. 21 (Springer, Berlin, 1991) p. 301.
[2] J.E. Black, in: Structure and Dynamics of Surfaces, Eds. W. Schommers and P. von Blankenhagen (Springer, Berlin, 1986) p. 153.
[3] J.A. Gasper and A.G. Eguiluz, Phys. Rev. B, 40 (1989) 11976.
[4] G.P. Alldredge, R.E. Allen and F.W. de Wette, Phys. Rev. B 4 (1971) 1682.
[5] R.E. Allen, G.P. Alldredge and F.W. de Wette, Phys. Rev. B 4 (1971) 1661.
[6] R.E. Allen, G.P. Alldredge and F.W. de Wette, Phys. Rev. B 4 (1971) 1648.
[7] G. Benedek and L. Miglio, in: Surface Phonons, Eds. W. Kress and F.W. de Wette (Springer, Berlin, 1991) p. 37.
[8] A. Rahman, Phys. Rev. 136 (1964) 405.
[9] C.Z. Wang, A. Fasolino and E. Tosatti, Phys. Rev. B 37 (1988) 2116.
[10] F. Ercolessi, M. Parrinello and E. Tosatti, Surf. Sci., 117 (1986) 314.
[11] F. Ercolessi, M. Parrinello and E. Tosatti, Philos. Mag. A 58 (1988) 213.
[12] X.Q. Wang, G.L. Chiarotti, F. Ercolessi and E. Tosatti, Phys. Rev. B 38 (1988) 8131.
[13] R.E. Allen, F.W. de Wette and A. Rahman, Phys. Rev. 179 (1969) 887.
[14] D. Gorse, J. Lapujoulade and V. Pontikis, Surf. Sci. 178 (1986) 434.
[15] B. Hall and D.L. Mills, Phys. Rev. B 40 (1989) 6326.
[16] D.D. Koleske and S.J. Sibener, J. Electron Spectrosc. Relat. Phenom. 54/55 (1990) 363.
[17] B. Wiesen, K.H. Weyrich and R. Siems, Phys. Rev. B 36 (1987) 3175.
[18] C.Z. Wang, C.T. Chan and K.M. Ho, Phys. Rev. B 40 (1989) 3390.
[19] J.D. Fan, O.A. Karim, G. Reiter and S.C. Moss, in: Computer Simulation Studies in Condensed Matter Physics, Eds. D.P. Landau, K.K. Mon and H. Schüttler (Springer, Berlin, 1988) p. 229.
[20] F.F. Abraham, Phys. Rev. Lett. 50 (1983) 978.
[21] U. Landman, W.D. Luedtke, R.N. Barnett, C.L. Cleveland, M.W. Ribarsky, E. Arnold, S. Ramesh, H. Baumgart, A. Martinez and B. Kahn, Phys. Rev. Lett. 56 (1986) 155.
[22] U. Landman, in: Computer Simulation Studies in Condensed Matter Physics, Eds. D.P. Landau, K.K. Mon and H. Schuttler (Springer, Berlin, 1988) p. 108.
[23] E.T. Chen, R.N. Barnett and U. Landman, Phys. Rev. B 41 (1990) 439.
[24] E.T. Chen, R.N. Barnett and U. Landman, Phys. Rev. B 40 (1989) 924.
[25] W.D. Luedtke and U. Landman, Phys. Rev. B 40 (1989) 11733.
[26] P. Stoltze, J.K. Nørskov and U. Landman, Phys. Rev. Lett. 61 (1988) 440.
[27] J.E. Black and P. Bopp, Surf. Sci. 140 (1984) 275.
[28] W.H. Press, B.P. Flannery, S.A. Teukolshy and W.T. Vetterling, Numerical Recipes (Cambridge University Press, Cambridge, 1986).
[29] A. Lock, J.P. Toennies and G. Witte, J. Electron Spectrosc. Relat. Phenom. 54/55 (1990) 309.
[30] P. Knipp, Phys. Rev. B 43 (1991) 6908.
[31] G. Armand and J.R. Manson, Phys. Rev. B 37 (1988) 4363.
[32] G. Armand and P. Zeppenfeld, Phys. Rev. B 40 (1989) 5936.
[33] G. Armand, D. Gorse, J. Lapujoulade and J.R. Manson, Europhys. Lett. 3 (1987) 1113.
[34] G. Armand, J.R. Manson and C.S. Jayanthi, Phys. Rev. B 34 (1986) 6627.
[35] A.P. Sutton and J. Chen, Philos. Mag. Lett. 61 (1990) 139.
[36] M.W. Finnis and J.E. Sinclair, Philos. Mag. A 50 (1984) 45.
[37] W. Schommers, in: Structure and Dynamics of Surfaces I, Eds. W. Schommers and P. von Blackenhagen (Springer, Berlin, 1986) p. 199.
[38] A.R. McGurn, A.A. Maradudin, R.F. Wallis and A.J.C. Ladd, Phys. Rev. B 37 (1988) 3964.
[39] W.E. Milne, Numerical Solutions of Differential Equations (Dover, New York, 1970).

[40] W.F. van Gunsteren and H.J.C. Berendsen, Mol. Phys. 34 (1977) 1311.
[41] M.L. Klein and T.R. Koehler, in: Rare Gas Solids, Eds. M.L. Klein and J.A. Venables (Academic Press, London, 1976) p. 301.
[42] R. Ravelo and M. El-Batanouny, Phys. Rev. B 40 (1989) 9574.
[43] A.A. Maradudin, E.W. Montroll, G.H. Weiss and I.P. Ipatova, Theory of Lattice Dynamics in the Harmonic Approximation (Academic Press, New York, 1971).
[44] R.E. Allen and F.W. de Wette, Phys. Rev. 179 (1969) 873.
[45] P.D. Ditlevsen, P. Stoltze and J.K. Nørskov, Phys. Rev. B (1991) submitted.
[46] Y. Chen, Z.Q. Wu, S.Y. Tong and J.E. Black, Surf. Sci. 210 (1989) 271.